Formation of robust and completely tunable resonant photonic band gaps

Shiyang Liu,[1,2] Junjie Du,[1,2] Zhifang Lin,[1,2] R. X. Wu,[3] and S. T. Chui[2]
[1]*Surface Physics Laboratory, Department of Physics, Fudan University, Shanghai 200433, People's Republic of China*
[2]*Bartol Research Institute, University of Delaware, Newark, Delaware 19716, USA*
[3]*Department of Electronic Sciences and Engineering, Nanjing University, Nanjing 210093, People's Republic of China*
(Received 11 June 2008; published 1 October 2008)

We examine the mechanism governing the photonic band gaps (PBGs) in two-dimensional magnetic photonic crystals consisting of ferrite cylinders, based on the simulation on the band structure and the transmission spectra. Besides the conventional PBG resulting from the Bragg scattering, two other types of PBGs, owing, respectively, to the Mie scattering resonance and the spin-wave resonance, are identified. Of particular interest is the PBG due to the Mie resonance that can be regarded as a magnetic analog of the surface plasmon in metal. The "magnetic surface plasmon" induced resonant PBGs is shown to be completely tunable by an external static magnetic field and robust against position disorder of the ferrite rods, in addition to possessing an analytically predictable PBG frequency.

DOI: 10.1103/PhysRevB.78.155101 PACS number(s): 42.70.Qs, 41.20.Jb, 42.25.Fx

I. INTRODUCTION

Since the pioneering work of Yablonovitch[1] and John,[2] photonic crystals (PCs) or photonic band gap (PBG) materials have attracted much attention and become the subject of intensive theoretical and experimental research because of their promising applications in micro- and optoelectronics.[3–5] One unique characteristic of PCs is the existence of PBGs, the frequency ranges over which all electromagnetic (EM) modes are forbidden, which enables the manipulation of the EM waves in many elaborately designed ways.

To achieve even more degrees of manipulability, tunable PCs have been proposed and investigated, where the photonic band structures or the PBGs can be modulated extrinsically. To obtain such tunable PCs, the permittivity and/or permeability of one or more constituents must depend on some external parameters such as electric field,[6–8] magnetic field,[9–12] temperature,[13,14] or strain.[15] In this work we shall concentrate on the effect of the external static magnetic field (ESMF) on the PBGs of the magnetic photonic crystal (MPCs), which includes the magnetic materials as one of its constituents.

As a typical tunable PC, the MPC has attracted a lot of interest[16–18] due to the fast switching time of magnetic systems, in addition to the potential tunability of the photonic band structure by the ESMF. However, there is still something left to be clarified, namely, how the PBGs are manipulated and to what extent they are tuned by the ESMF. Furthermore, whether or not all the PBGs appearing in the photonic band structures could be tuned, even further, what is the mechanism behind the tunability of PBGs in the MPCs.

In this paper we demonstrate that even though not all PBGs are easily tunable, there exist PBGs that can be easily manipulated by the ESMF in the PC composed of ferrites, a typical MPC. By examining the mechanism dominating the PBGs in the ferrite-based MPC, we identify three different types of PBGs, which arise, respectively, from (1) the Bragg scattering, (2) the Mie scattering resonance of an individual ferrite cylinder that is a magnetic analog of a surface plasmon in metal,[19] and (3) the spin-wave resonance. The responses of different PBGs to the ESMF diverge substantially. While our results show that the conventional PBG owing to the Bragg scattering in the ferrite-based MPC behave quite inertly in response to the ESMF, the latter two types of PBGs resulting from resonance of individual scatterer are sensitively tunable by the ESMF and, in particular, their frequencies are analytically predictable. In addition, the resonant types of PBG are robust against the position disorder of the magnetic scatterers.

The paper is organized as follows: In Sec. II we examine the mechanisms dominating the PBG in a MPC composed of ferrite rods, as well as the magnetic tunability of the PBGs. Then in Sec. III the simulation on transmission coefficients is performed, mainly to show the physical consequence of the tunability of the PBGs and study the influence of position disorder on different PBGs. Finally, a summary is given in Sec. IV.

II. PHOTONIC BAND STRUCTURE OF MPC

We exemplify our study on the band structure of the ferrite-based MPC by a two-dimensional (2D) hexagonal lattice of ferrite rods in a nonmagnetic Plexiglas background, with the lattice constant a and all rod axes along the z direction. When fully magnetized, the ferrite has the magnetic permeability tensor in gyromagnetic form[20]

$$\hat{\mu} = \begin{pmatrix} \mu_r & -i\mu_\kappa & 0 \\ i\mu_\kappa & \mu_r & 0 \\ 0 & 0 & 1 \end{pmatrix}, \tag{1}$$

with

$$\mu_r = 1 + \frac{\omega_m(\omega_0 - i\alpha\omega)}{(\omega_0 - i\alpha\omega)^2 - \omega^2}, \quad \mu_\kappa = \frac{\omega_m\omega}{(\omega_0 - i\alpha\omega)^2 - \omega^2},$$

where $\omega_0 = \gamma H_0$ is the resonance frequency with γ the gyromagnetic ratio, H_0 is the sum of the ESMF applied in the z direction and the shape anisotropy field,[20] $\omega_m = 4\pi\gamma M_s$ is the characteristic frequency with $4\pi M_s$ the saturation magneti-

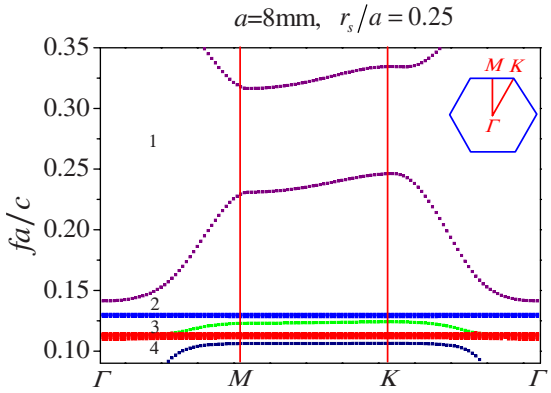

FIG. 1. (Color online) The photonic band structure of a 2D hexagonal lattice of ferrite rods, with $a=8$ mm, $r=2$ mm, and $H_0=900$ Oe. The reduced Brillouin zone is displayed in the inset together with the high-symmetry points. Four PBGs are labeled by 1, 2, 3, and 4, from higher to lower frequency.

zation, and α is the damping coefficient of the ferrite. In our band-structure calculation, we set $\alpha=0$.[21]

In the 2D EM systems, the transverse electric (TE) mode and the transverse magnetic (TM) mode are independent eigenmodes and can be studied separately. For the TE mode, the magnetic field of the EM wave is polarized along the z direction, parallel to the ESMF, implying a constant permeability. Consequently, the tunability of the ESMF works only for the TM mode, where the magnetic field of the EM wave is normal to the ESMF, resulting in the precessing of the magnetic dipoles in the ferrite. For this reason only the TM mode is tunable by the ESMF and will be considered here.

Most photonic band-structure calculations have been based on the plane-wave expansion method[22] or the finite difference time domain method.[23] However, for dispersive systems with gyromagnetic scatterers, it is rather difficult to achieve a reliable convergence of the solutions. In particular, sometimes the plane-wave expansion method may produce unreliable results.[24] For PCs consisting of nonoverlap spheres or circular cylinders, the multiple-scattering method (MSM) proves to be most powerful,[17,24–26,31] provided that the scattering matrix for individual scatterers can be obtained exactly. Accordingly, in this paper, the MSM incorporated with the exact scattering matrix for a 2D gyromagnetic rod[17,27] is employed in the photonic band-structure calculation and transmission spectra simulation.

The photonic band structure for a hexagonal lattice of ferrite rods is typically shown in Fig. 1 for $H_0=900$ Oe, where the lattice constant is taken as $a=8$ mm, and the radius of the ferrite cylinder is $r_s=\frac{1}{4}a=2$ mm. The relative permittivity and permeability of the nonmagnetic background medium (Plexiglas) are $\epsilon_m=2.6$ and $\mu_m=1$. For the ferrite cylinder $\epsilon_s=12.3$ and the saturation magnetization $4\pi M_s=1700$ gauss, typical for yttrium iron garnet (YIG) ferrite.[20] The reduced Brillouin zone is illustrated as well in the inset. The corresponding high-symmetry points are $\Gamma=\frac{2\pi}{a}(0,0)$, $M=\frac{2\pi}{a}(0,\frac{1}{\sqrt{3}})$, and $K=\frac{2\pi}{a}(\frac{1}{3},\frac{1}{\sqrt{3}})$. The frequency has been reduced by factor c/a with c the speed of light in vacuum. It is seen that in the band structure there exist four PBGs centered at $fa/c=0.275$, 0.138, 0.130, and 0.108, labeled by 1, 2, 3, and 4, respectively, as shown in Fig. 1. We will examine the origin and the tunability by the ESMF of these PBGs below.

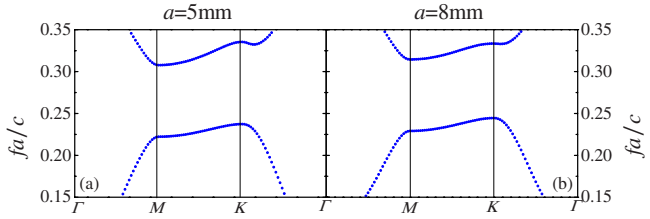

FIG. 2. (Color online) (a) The photonic band structure near the first PBG of a 2D hexagonal lattice of ferrite rods, with $a=5$ mm and $r_s=\frac{1}{4}a$ while all other parameters the same as those in Fig. 1. (b) An amplified part near the first PBG of Fig. 1. Scaling behavior is obvious and the first PBG manifests itself as a conventional PBG owing to the multiple Bragg scattering.

Let us first focus on the first PBG centered at $fa/c=0.275$. To elucidate the mechanism of this PBG, we present in Fig. 2 the amplified part of the band structure around this PBG [Fig. 2(b)], together with the band structure [Fig. 2(a)] for a scaled system with $a=5$ mm while keeping the filling fraction and all other parameters unchanged. It is found that the PBG is centered at almost the same position when the frequency is in units of c/a. In addition, the photonic band structures around the PBG are nearly the same, showing a pretty good scale-length invariant behavior. It is therefore concluded that the first PBG is a conventional one dominated by the Bragg scattering.

To illustrate the effect of the ESMF on this PBG, we have calculated the band structures with the application of different ESMFs. The results are typically shown in Fig. 3 for $H_0=700$ Oe (a) and $H_0=900$ Oe (b), while keeping all other parameters the same as in Fig. 1. Figure 3(b) is actually an amplified part of Fig. 1 presented together for comparison. It can be found that the two band structures with different ESMFs are nearly the same, suggesting that the ESMF has little effect on the first PBG and the photonic band structure nearby. This explains the recent experimental results[18] that show a tiny shift in frequency of the PBGs in response to the change of the ESMF. Consequently, it appears hard to manipulate the conventional PBG with the ESMF.

Next, let us look at the second PBG centered at $fc/a=0.138$, as labeled by 2 in Fig. 1. To illustrate the effect of the ESMF, we show in Fig. 4(a) the photonic band structures

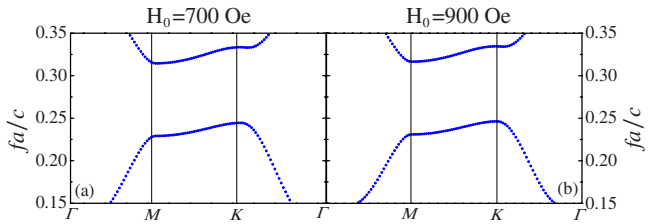

FIG. 3. (Color online) (a) The photonic band structure near the first PBG of a 2D hexagonal lattice of ferrite rods, with $H_0=700$ Oe and all other parameters the same as those in Fig. 1. (b) An amplified part near the first PBG of Fig. 1. The inert response of the PBG to the ESMF manifests.

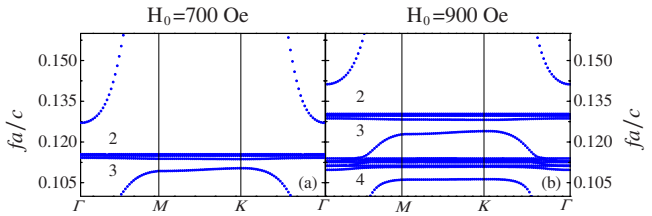

FIG. 4. (Color online) (a) The photonic band structure near the second and third PBGs of a 2D hexagonal lattice of ferrite rods, with $H_0=700$ Oe and all other parameters the same as those in Fig. 1. (b) An amplified part of Fig. 1. Numbers in the figure label the indices of the PBGs as shown in Fig. 1. The effect of ESMF on the band structure manifests.

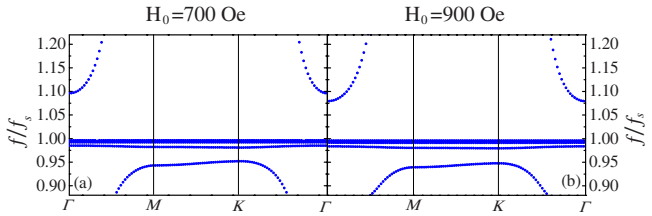

FIG. 5. (Color online) Replot of the photonic band structure of Fig. 4 with frequency in units of the magnetic surface-plasmon frequency f_s given by Eq. (2).

near the second PBG for a system with $H_0=700$ Oe and all other parameters the same as in Fig. 1. Also shown in Fig. 4(b) is an amplified part of Fig. 1 (with $H_0=900$ Oe) for the purpose of comparison. Different from the first PBG, a significant change of band structure can be observed in Fig. 4. An increase of the ESMF makes the second PBG move upward substantially, so do the third and fourth PBGs. An important characteristic to be noted from Fig. 4 is that there exist dense sets of flat bands between the second and the third PBGs (see also the blue bands in Fig. 1), signifying the occurrence of some kind of resonance.

In the study of plasmonics,[19] flat photonic bands have been observed near the surface plasmon frequency[28] with $\epsilon=-1$ in 2D and $\epsilon=-2$ in three dimensions (3D). In our case flat bands occur when the effective magnetic susceptibility $\mu_r+\mu_\kappa=-1$, which can be considered as the magnetic analog of the surface plasmon in metal. Indeed, from our dispersive permeability in Eq. (1), it can be derived that $\mu_r+\mu_\kappa=-1$ at the frequency

$$f_s=\frac{1}{2\pi}\left(\omega_0+\frac{1}{2}\omega_m\right). \tag{2}$$

Consequently, the frequency of the flat bands can be tuned by ESMF, while for the flat bands resulting from conventional surface-plasmon resonance the corresponding frequency is not manipulable.[28] For the MPC under investigation, with $4\pi M_s=1700$ gauss and $a=8$ mm, we have $f_s a/c=0.1158$ and 0.1308 for $H_0=700$ Oe and $H_0=900$ Oe, respectively. From Fig. 4 it can be seen clearly that f_s is on top of the set of flat bands, above and below which open up the second and third PBGs, respectively.

Physically, $\mu_{\text{eff}}=\mu_r+\mu_\kappa=-1$ ($\epsilon=-1$) corresponds to the Mie resonance of all angular momenta $n<0$ of a 2D circular cylinder for TM (TE) modes in the long wavelength limit. We found analytically[29] that this corresponds to an infinite number of degenerate flat bands in the limit $x=\omega r_s/c\to 0$. For finite but small x, one has an infinite number of densely packed flat bands just below f_s. A detailed study of these flat bands and their physical implications will be published elsewhere.

The above analysis suggests that the frequency f_s, which is completely manipulable by the ESMF through ω_0, determines the positions of the second and the third PBGs. To corroborate this, we have replotted in Fig. 5 the photonic band structures in Fig. 4 with the eigenfrequencies normalized by f_s. The location of frequency $f/f_s=1$ corresponds to the top of the flat bands lying between the second and the third PBGs. This illustrates the effect of the ESMF in moving the frequency of the PBG through shifting the value of f_s.

To verify that the second and third PBGs have nothing to do with the Bragg scattering, we have studied the band structure for systems with the lattice constants scaled by a variety of factors. Typical results are shown in Fig. 6, where we fixed $H_0=700$ Oe and scaled the system from $a=5$ mm [Fig. 6(a)] to $a=8$ mm [Fig. 6(b)], while keeping the filling fraction and all other parameters the same as in Fig. 1. For the convenience of comparison the unit of the frequency is taken as gigahertz. It can be found that although the lattice constants are different the flat bands between the second and the third PBGs are located at the same frequency for Figs. 6(a) and 6(b). This demonstrates the independence of the flat bands on the lattice constant and rules out the possibility of the Bragg scattering mechanism. The position of the flat bands is solely determined by f_s and therefore depends on the ESMF and the saturation magnetization only. As a consequence, it can be expected that the second and the third PBGs will be robust and persistent against the position disorder in ferrite rods, while the first conventional PBG, although much wider, will be ruined by the position disorder. This will be corroborated in Sec. III by the transmission spectra.

Finally, we turn to the fourth PBG in Fig. 1, above which appears also a dense set of flat bands, as exhibited by red bands, implying once again some kind of resonance. The frequency of these flat bands can also be tuned by the ESMF, as shown in Fig. 4. These flat bands have their origin from the spin-wave resonance. From Eq. (1), it can be found that

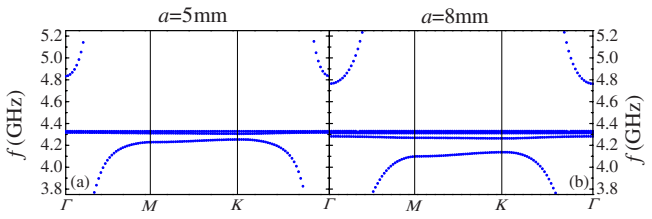

FIG. 6. (Color online) The photonic band structure near the second and third PBGs of a 2D hexagonal lattice of ferrite rods with (a) $a=5$ mm and (b) $a=8$ mm, exhibiting the independence of the PBG frequency on the lattice constant a. The applied ESMF is such that $H_0=700$ Oe while all other parameters are the same as those in Fig. 1.

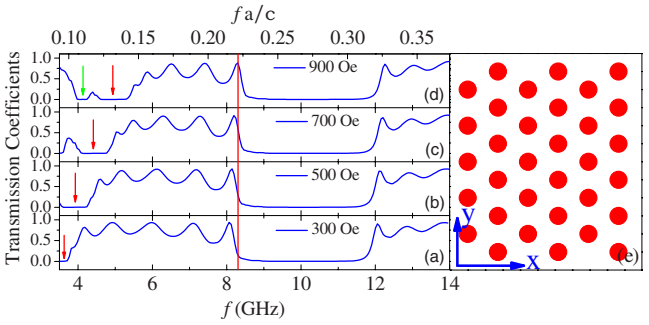

FIG. 7. (Color online) Transmission coefficients of the hexagonal MPC sample for (a) $H_0=300$ Oe, (b) 500 Oe, (c) 700 Oe, and (d) 900 Oe. The lattice constant is $a=8$ mm and the radius of the ferrite cylinder is $r_s=\frac{1}{4}a=2$ mm. The red (green) arrows denote the positions of second and third (fourth) PBGs. The red vertical line serves as a guide to the eyes, showing that the first PBG is shifted by only a small amount with the change of ESMF. On the right panel (e) is a schematic illustration of the sample considered.

$\mu_r=\mu_r'=0$ at a frequency $f_m=\frac{1}{2\pi}\sqrt{\omega_0(\omega_0+\omega_m)}$, where $\mu_r'=\mu_r/(\mu_r^2-\mu_\kappa^2)$. As a result, the wave vector inside the ferrite cylinder, which is proportional to $1/\sqrt{\mu_r'}$, tends to infinity at frequency f_m, corresponding to the occurrence of the "spin-wave resonance." For our system with $H_0=900$ Oe, we have $f_m=0.114c/a$, which corresponds to the top of the flat bands, as shown in Fig. 4(b). The frequency of the fourth PBG can therefore be tuned by the ESMF through the modulation of f_m, in a similar way to the manipulation of the second and third PBGs through f_s.

III. SIMULATION ON TRANSMISSION COEFFICIENTS

To demonstrate the physical consequence due to the tunability of the PBGs, we have performed simulations on the transmission coefficients, which can be expressed as the forward-scattering amplitude of the MPC.[30] Different from the photonic band-structure calculation, in this section we adopt the practical material parameters and take into account the weak absorption of the sample. In our simulation the relative permittivities of the nonmagnetic background medium and the ferrite cylinder are taken as $\epsilon_b=2.6+i0.005$ and $\epsilon_s=12.3+i0.0006$, respectively.[18] The relative permeability is $\mu_b=1.0$ for background medium and that of the ferrite cylinder is given in Eq. (1) with the damping coefficient taken as $\alpha=0.007$.[20]

Typical results of the transmission for different values of H_0 are shown in Fig. 7. The sample considered is a seven-layer structure with the surface normal of the layer along the x direction. The configuration is schematically displayed in Fig. 7(e). The lattice constant is $a=8$ mm and the radius of the ferrite cylinder is $r_s=\frac{1}{4}a$. For convenience, the frequency is given both in units of gigahertz (bottom) and in c/a (top). It can be seen from Fig. 7 that with the increase of the ESMF the second, the third (denoted by the red arrows), and the fourth PBGs (denoted by the green arrow) shift significantly to higher frequencies. However, the first PBG arising from the Bragg scattering shows only a tiny shift in the frequency when H_0 is varied from 300 to 900 Oe, as manifested in Fig. 7 by the red vertical line serving as a guide to eyes for the low-frequency edge of the first PBG. The gap of the transmission coefficients is in quantitative agreement with those obtained in the photonic band structures. For example, in Fig. 7(d) the middle gap frequency of the first PBG is about $0.275c/a$, which is the same as that in the photonic band-structure calculation. The second transmission gap (denoted by the red arrows) comes from the second PBG, the third PBG, and the flat bands (blue bands in Fig. 1) that induce null transmission. The middle frequency is $0.135c/a$, which is also the middle frequency of the corresponding part in the photonic band structure. The third transmission gap (denoted by the green arrow) results from the fourth PBG and corresponding flat bands (red part in Fig. 1). The middle frequency $0.125c/a$ is in agreement with that of the corresponding band structure as well. The transmission between the second and the third transmission gap corresponds to the band between two sets of flat bands as shown in green in Fig. 1. In Fig. 7 we find some oscillations of the transmission coefficients in the frequency range between the first and the second gaps. This is due to the finite size of the sample, as pointed out by Stefanou *et al.*[31]

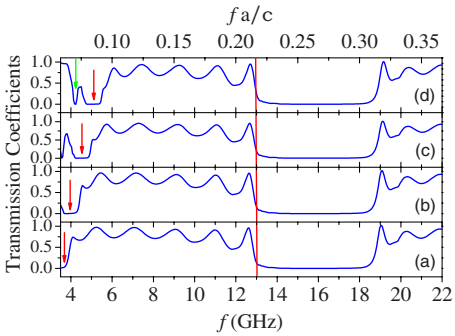

FIG. 8. (Color online) The same as Fig. 7 except that the lattice constant is $a=5$ mm and the radius of the ferrite cylinder is $r_s=\frac{1}{4}a=1.25$ mm, keeping the filling fraction unchanged.

In the photonic band-structure calculation, it is found that the position of the first PBG, which results from the Bragg scattering, scales with the lattice constant a, while the second and the third PBGs, which have their origin from the Mie scattering resonance of the individual scatterers, show little dependence on a. This is verified further by our simulation on the transmission. In Fig. 8 we show the transmission coefficient for a system with the lattice constant $a=5$ mm while keeping the filling fraction and all other parameters the same as in Fig. 7. Because the lattice constant is scaled from $a=8$ mm to $a=5$ mm, the center frequency of the first PBG has moved from 10 to 16 GHz. In the reduced unit c/a, the position of the center frequency of the first PBG stays at $0.275c/a$, the same as that in Fig. 7. This is in agreement with the photonic band-structure calculation. The center frequency of the second transmission gap remains almost the same as that in Fig. 7 at different ESMFs, in agreement with the results in Fig. 6. The simulation on the transmission confirms the conclusions obtained from photonic band-structure calculation.

From Sec. II, we know that the second and the third PBGs arise from the "magnetic surface-plasmon" resonance of the

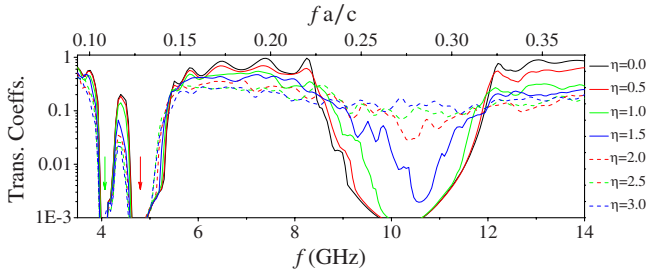

FIG. 9. (Color online) Transmission coefficients of the sample with the introduction of different degree of disorder characterized by η. The lattice constant is 8 mm and the radius of the ferrite cylinder is $r_s=\frac{1}{4}a=2$ mm. The applied ESMF is such that $H_0=900$ Oe. The red and green arrows denote the robust transmission gaps.

individual ferrite cylinder. They show little dependence on the lattice constant. It is natural to expect that the PBGs are robust against the position disorder of ferrite rods. This is corroborated by our simulation on the transmission, where disorder can be introduced to the positions of the ferrite cylinders. Within a unit cell the maximum variations of the position of the ferrite cylinder along x and y directions are, respectively, $d_{x0}=\frac{\sqrt{3}}{2}a-2r$ and $d_{y0}=a-2r$. [See Fig. 7(e) for a schematic illustration of the MPC.] The displacement of each cylinder from the position in the perfect hexagonal lattice can be defined as $d_i=\xi\ \eta\ d_{i0}$ with $i=x$ or y and ξ a random number uniformly distributed between −0.5 and 0.5. Here η is a parameter introduced to measure the degree of disorder. $\eta=0$ corresponds to the case that no disorder is introduced, $\eta<1$ denotes the case where the displacement is restricted within each unit cell, and $\eta>1$ means the maximum variations of the position can be beyond the unit cell. We have made some further adjustments to avoid the overlap of the ferrite cylinders for the case with $\eta>1$.

In Fig. 9 the results of the transmission coefficients with different randomness η are presented. The corresponding parameters are the same as in Fig. 7 except that H_0 is fixed at 900 Oe. Two kinds of units are shown as in Fig. 7 for the convenience of comparison. The results shown in Fig. 9 are the average over 20 realizations of the disordered system. The simulation is performed for η ranging from 0.5 to 3.0. The result for the sample without disorder ($\eta=0$) is also shown in solid black line for comparison. It can be seen that there exists no obvious change in the transmission coefficient when the disorder is very weak. With the increase of the randomness the first PBG becomes narrower and narrower and disappears eventually due to the breakdown of the Bragg scattering. However, the resonance-induced PBGs (regimes denoted by the red and green arrows) remain essentially unchanged. We conclude that the introduction of the positional disorder affects only the Bragg type of PBG significantly, while the other two types of PBGs, arising from resonance of individual scatterers, are quite robust against the position disorder. The similar effect has also been demonstrated in the research on optical properties of the system consisting of electric active entities.[32] However, it is pointed out that our results are the magnetic counterpart of the electric active entities and the more favorable aspect is that the property appearing in our system can be manipulated by ESMF.

IV. CONCLUSION

In summary, we have investigated the origin of the PBGs in a hexagonal lattice of ferrite rods based on the calculation of the photonic band structure as well as the transmission spectra. Three different types of PBGs are identified. They originated, respectively, from (1) the Bragg scattering, (2) the Mie scattering resonance of the individual ferrite cylinder that mimics the surface-plasmon resonance in the metallic counterpart, and (3) the "spin-wave resonance" of individual ferrite. The locations of the flat bands and therefore the PBGs that arise from the magnetic surface-plasmon resonance are presented analytically. An ESMF has only a weak effect on the PBG that stems from the Bragg scattering, while for the PBGs due to the resonance of individual scatterers, the gap frequency range can be manipulated effectively by an ESMF. In addition, while the PBG induced by Bragg scattering is sensitive to position disorder, as expected, the PBG due to the Mie scattering resonance or the magnetic surface-plasmon resonance shows rather robust behavior to position disorder and, consequently, provides robust and completely tunable resonant PBGs.

ACKNOWLEDGMENTS

This work was supported by CNKBRSF, NNSFC, PCSIRT, MOE of China (B06011), and Shanghai Science and Technology Commission. S.T.C. is partly supported by the U.S. DOE.

[1] E. Yablonovitch, Phys. Rev. Lett. **58**, 2059 (1987).
[2] S. John, Phys. Rev. Lett. **58**, 2486 (1987).
[3] J. D. Joannopoulos, R. D. Meade, and J. N. Winn, *Photonic Crystals* (Princeton University Press, Princeton, NJ, 1995).
[4] C. M. Soukoulis, *Photonic Band Gaps and Localization*, Proceedings of the NATO ARW (Plenum, New York, 1993).
[5] C. M. Soukoulis, *Photonic Band Gap Materials*, Proceedings of the NATO ASI (Kluwer, Dordrecht, 1996).
[6] K. Busch and S. John, Phys. Rev. Lett. **83**, 967 (1999).
[7] Q. B. Meng, C. H. Fu, S. Hayami, Z. Z. Gu, and O. Sato, J. Appl. Phys. **89**, 5974 (2001).
[8] D. Kang, J. E. Maclennan, N. A. Clark, A. A. Zakhidov, and R. H. Baughman, Phys. Rev. Lett. **86**, 4052 (2001).
[9] A. Figotin, Y. A. Godin, and I. Vitebsky, Phys. Rev. B **57**, 2841 (1998).
[10] M. Golosovsky, Y. Saado, and D. Davidov, Appl. Phys. Lett. **75**, 4168 (1999).
[11] C. S. Kee, J. E. Kim, H. Y. Park, I. Park, and H. Lim, Phys. Rev.

B **61**, 15523 (2000).
[12] H. P. Tian and J. Zi, Opt. Commun. **252**, 321 (2005).
[13] P. Halevi and F. Ramos-Mendieta, Phys. Rev. Lett. **85**, 1875 (2000).
[14] C. S. Kee and H. Lim, Phys. Rev. B **64**, 121103(R) (2001).
[15] S. Kim and V. Gopalan, Appl. Phys. Lett. **78**, 3015 (2001).
[16] M. M. Sigalas, C. M. Soukoulis, R. Biswas, and K. M. Ho, Phys. Rev. B **56**, 959 (1997); E. D. V. Nagesh, V. Subramanian, V. Sivasubramanian, and V. R. K. Murthy, Physica B (Amsterdam) **382**, 45 (2006); I. L. Lyubchanskii, N. N. Dadoenkova, M. I. Lyubchanskii, E. A. Shapovalov, and Th. Rasing, J. Phys. D **36**, R277 (2003); W. L. Jia, Y. Z. Li, Y. G. Xi, P. Jiang, X. H. Xu, X. H. Liu, R. T. Fu, and J. Zi, J. Phys.: Condens. Matter **15**, 6731 (2003); M. Inoue, R. Fujikawa, A. Baryshev, A. Khanikaev, P. B. Lim, H. Uchidal, O. Aktsipetrov, A. Fedyanin, T. Murzina, and A. Granovsky, J. Phys. D **39**, R151 (2006); S. T. Chui and Z. Lin, J. Phys.: Condens. Matter **19**, 406233 (2007).
[17] Z. F. Lin and S. T. Chui, Opt. Lett. **32**, 2288 (2007).
[18] J. Xu, R. X. Wu, P. Chen, and Y. Shi, J. Phys. D **40**, 960 (2007); P. Chen, R. X. Wu, J. Xu, A. M. Jiang, and X. Y. Ji, J. Phys.: Condens. Matter **19**, 106205 (2007).
[19] A. V. Zayats, I. I. Smolyaninov, and A. A. Maradudin, Phys. Rep. **408**, 131 (2005).
[20] D. M. Pozar, *Microwave Engineering*, 3rd ed. (Wiley, New York, 2004).
[21] Single-crystal YIG can have a linewidth as low as 0.3 Oe, corresponding to $\alpha \sim 10^{-4}$. The dielectric loss tangent tan δ is of order of 10^{-4}, see Ref. 19, allowing neglect of damping; see, e.g., Z. Wang, Y. D. Chong, J. D. Joannopoulos, and M. Soljačić, Phys. Rev. Lett. **100**, 013905 (2008).
[22] K. M. Ho, C. T. Chan, and C. M. Soukoulis, Phys. Rev. Lett. **65**, 3152 (1990).
[23] C. T. Chan, Q. L. Yu, and K. M. Ho, Phys. Rev. B **51**, 16635 (1995).
[24] A. Moroz, Phys. Rev. B **66**, 115109 (2002).
[25] Z. Lin and S. T. Chui, Phys. Rev. E **69**, 056614 (2004).
[26] S. Liu and Z. Lin, Phys. Rev. E **73**, 066609 (2006).
[27] W. H. Eggimann, IEEE Trans. Microwave Theory Tech. **8**, 440 (1960).
[28] V. Yannopapas, A. Modinos, and N. Stefanou, Phys. Rev. B **60**, 5359 (1999); A. R. McGurn and A. A. Maradudin, *ibid.* **48**, 17576 (1993); V. Kuzmiak, A. A. Maradudin, and F. Pincemin, *ibid.* **50**, 16835 (1994).
[29] S. T. Chui, Z. F. Lin, and L. Zhou (unpublished).
[30] L. M. Li and Z. Q. Zhang, Phys. Rev. B **58**, 9587 (1998).
[31] N. Stefanou, V. Yannopapas, and A. Modinos, Comput. Phys. Commun. **113**, 49 (1998).
[32] A. Modinos, V. Yannopapas, and N. Stefanou, Phys. Rev. B **61**, 8099 (2000); Z. L. Wang, C. T. Chan, W. Y. Zhang, N. B. Ming, and P. Sheng, *ibid.* **64**, 113108 (2001); V. Yannopapas and N. V. Vitanov, *ibid.* **74**, 193304 (2006).